AIAA-2016-2887

22nd AIAA/CEAS Aeroacoustics Conference, 31 May – 01 June 2016, Lyon, France

An asymptotic model for non-linear Helmholtz resonator of finite depth

Sjoerd W. Rienstra* and Deepesh Kumar Singh†

Department of Mathematics and Computer Science, TU Eindhoven, The Netherlands

The nonlinear corrections for a Helmholtz resonator type impedance based on systematic asymptotic solution of the pertaining equations has been formulated in [1]. The length of the cavity considered was much smaller compared to the typical acoustic wavelength of interest so that the pressure inside could be assumed to be uniform. This way, the cavity worked as a spring to the external excitation and the velocity obtained was given by the time derivative of the uniform pressure. In the current work, this model is refined to take into account the development of the standing waves inside the cavity so that the model captures more physics of the damping phenomenon inside the cavity. We aim to present a systematic derivation (from first principles) of solution of the nonlinear Helmholtz resonator equation with the neck connected to an organ pipe type long cavity to have the acoustic waves developed inside, in order to obtain analytically, an expression for the impedance close to resonance, while including nonlinear effects. The amplitude regime is considered such that when we stay away from the resonance condition, the nonlinear terms are relatively small and the solution obtained is of the linear equation formed after neglecting the nonlinear terms. Close to the resonance frequency, the nonlinear terms can no longer be neglected and algebraic equations are obtained that describe the corresponding nonlinear impedance. Apart from a confirmation of the previously published impedance results [1], a better comparison with experimental data and the asymptotic matching of the linear and nonlinear impedance regimes is established.

I. Introduction

The sound emission from aircraft engines, power machines and several other industrial applications is a matter of high concern that affects the community noise and hence health and life. In most of the applications, the emission spectrum is concentrated near a few prominent frequencies that are in general attenuated with the help of liners. An important type of acoustic liner for aero-engine inlet and exhaust ducts constitutes of a honeycomb array of small cells called Helmholtz resonators. The Helmholtz resonator is a cavity filled with air and having a small opening called the neck. When excited with a fluctuating external pressure, the mass of the air plug inside the neck moves against the large volume of compressible air inside the cavity, which acts as a spring, while viscous forces and vortex shedding cause dissipation of energy. Altogether this establishes a mass-spring-damper system. The damping is normally relatively small such that a resonance frequency can be identified. At and near resonance, the dissipation is largest and so narrow band sound absorption is achieved for frequencies close to resonance. Properties of this process form the basic design criterion for the liners. The resonator, as "seen" from outside, is characterized by its impedance $Z = Z(\omega)$, relating (spatially averaged) pressure and velocity at the wall. Ideally, Z is a wall property, independent of the acoustic field. However, in particular near resonance, Z is amplitude dependent for high but relevant amplitudes, for example of the "buzz

*Associate Professor, Dept. Math. & Comp. Sc., Eindhoven Univ. of Techn., Netherlands, Senior Member AIAA.

†Doctoral candidate, Dept. Mathematics & Computer Science, Eindhoven University of Technology, Netherlands.

saw" noise in a turbofan engine due to the shocks produced in front of the fan at take off and the blade tips operating near sonic conditions [2, 3]. It is important to know quantitatively and understand qualitatively such impedances Z with good precision to improve the design of the structures to have the highest possible attenuation of the emitted soundfield.

The nonlinear effects are mainly of hydrodynamical origin, due to the resistive losses and vortex shedding at inflow/outflow from the opening as shown in Fig. 2. This is physically a process of great complexity [4, 5] which has indeed exacerbated the possibility to obtain the impedance with an accurate model based on first principles.

The nonlinear corrections of the impedance, common in the literature, are based on physically inspired modelling assumptions, but otherwise do not aim to solve the equations of the nonlinear resonator [6, 7, 8]. In contrast, the properties of the Helmholtz resonator have been obtained from the full equations in [2, 9, 10, 11, 12, 13, 14], but these are all fully CFD, DNS or LES simulations which do not give information for the simpler models. The Helmholtz resonator equation which describes the neck region flow (Fig. 1) can be solved asymptotically with the boundary condition that relates the pressure and velocities inside the cavity (left of the neck in Fig. 1). This was done in [1] and the formulated impedance was compared with the existing experimental data favourably. The considered cavity was acoustically compact, *i.e.* the length of the cavity considered was much smaller compared to the acoustic wavelength $L \ll \lambda$ so that the pressure inside was nearly uniform and the neck velocity was simply given by the time derivative of the pressure. Hence the resonator acts like a spring to the external force. This modelling assumption could be improved and extended to cavities of finite lengths by solving the wave equation inside the cavity to obtain a relationship between pressure and velocity of the waves developing inside the cavity. In this way, we capture more physics of the problem and the fidelity of the model is improved.

We follow much of the derivation done in [1], and focus on a systematic derivation of an asymptotic solution of a stand-alone nonlinear Helmholtz resonator equation from first principles. The extra complication of grazing flow along the liner wall will not be considered here. This effect is important if the mean flow boundary layer is thin enough and the resonator outflow velocity is comparable to (or higher than) the mean flow velocity.

We start with the classical modelling of the Helmholtz resonator and formulate a perturbation problem in terms of a small parameter ε which is based on the excitation amplitude of a given pressure of fixed frequency. The stationary solution of this problem is solved asymptotically. Secular effects of the external forcing are treated in the usual way by a suitable Lindstedt-Poincaré type approach. A non-standard problem is the modulus term $|u|$ of the velocity. This prohibits a standard asymptotic expansion because the location of the zeros of u are a priori unknown. This problem has been tackled by adding an unknown shift of the origin, to be determined along with the construction of the solution, and using the fact that the stationary solution has the same periodicity as the driving force.

II. Mathematical formulation

The organ-pipe type resonator, that is considered here, is shown in Fig 1. The base area of the cavity of length L is S_b and the cross sectional area of the neck is S_n. It should be noted that this neck area is to be interpreted as the *effective* cross section. In other words, the geometric cross section multiplied by a discharge coefficient, to include what is commonly known as the *vena contracta* effect (due to separation of the streamlines at the opening edge). This will normally be a weak function of the amplitude, but is assumed to be constant here.

The frequency of the external excitation is assumed to be low enough that crosswise higher order modes are cut off in the cavity region of length L, leading to only plane waves inside. Considering that the cavity neck is acoustically compact *i.e.* $k\ell \ll 1$ for a typical wavenumber $k = \omega/c_0$, we can neglect compressibility in the neck and determine the line integral of the momentum equation

$$\rho_0\Big(\frac{\partial \boldsymbol{v}}{\partial t} + \boldsymbol{v}\cdot\nabla\boldsymbol{v}\Big) + \nabla p = \mu\nabla^2\boldsymbol{v}$$

along a streamline from a point inside to a point outside to obtain the relation

$$\rho_0 \int_{\text{in}}^{\text{ex}} \frac{\partial \boldsymbol{v}}{\partial t} \cdot \mathbf{d}\boldsymbol{s} + \tfrac{1}{2}\rho_0(v_{\text{ex}}^2 - v_{\text{in}}^2) + (p_{\text{ex}} - p_{\text{in}}) = \int_{\text{in}}^{\text{ex}} \mu \nabla^2 \boldsymbol{v} \cdot \mathbf{d}\boldsymbol{s}, \tag{1}$$

with $v = \|\boldsymbol{v}\|$ and μ denoting the viscosity. Following Melling [6] we average pressure and velocity along the neck's cross section, assume that the averaged squared velocity is approximately equal to the squared averaged velocity, and obtain

$$\rho_0 \int_{\text{in}}^{\text{ex}} \frac{\partial \overline{\boldsymbol{v}}}{\partial t} \cdot \mathbf{d}\boldsymbol{s} + \tfrac{1}{2}\rho_0(\overline{v}_{\text{ex}}^2 - \overline{v}_{\text{in}}^2) + (p_{\text{ex}} - p_{\text{in}}) = \int_{\text{in}}^{\text{ex}} \mu \overline{\nabla^2 \boldsymbol{v}} \cdot \mathbf{d}\boldsymbol{s}. \tag{2}$$

Assuming that the streamline does not change in time, we have

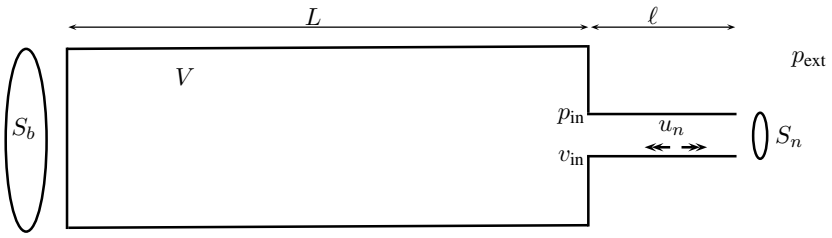

Figure 1. Organpipe resonator cavity and neck

$$\int_{\text{in}}^{\text{ex}} \frac{\partial \overline{\boldsymbol{v}}}{\partial t} \cdot \mathbf{d}\boldsymbol{s} = \frac{\mathrm{d}}{\mathrm{d}t} \int_{\text{in}}^{\text{ex}} \overline{\boldsymbol{v}} \cdot \mathbf{d}\boldsymbol{s}. \tag{3}$$

The velocity line integral evidently scales on a typical length times a typical velocity. If end effects are minor, we can use the neck flux velocity $\overline{\boldsymbol{v}} = u_n \boldsymbol{e}_x$ with a corresponding length being the neck length ℓ, added by a small end correction δ to take into account the inertia of the acoustic flow at both ends just outside the neck (inside and outside the resonator). Then we have

$$\int_{\text{in}}^{\text{ex}} \overline{\boldsymbol{v}} \cdot \mathbf{d}\boldsymbol{s} = (\ell + 2\delta) u_n. \tag{4}$$

End corrections δ for various geometries are given by Ingard [15]. For a circular orifice, for example, we may use $\delta = 0.85(S_n/\pi)^{1/2}$.

For the stress term line integral we observe that, apart from u_n itself, it will depend on flow profile, Reynolds number, wall heat exchange, turbulence, separation from sharp edges, and maybe more. Following Melling [6], we will take these effects together in a resistance factor R, which will be assumed relatively small, in order to have resonance and a small decay per period to begin with. We thus have

$$\int_{\text{in}}^{\text{ex}} \mu \overline{\nabla^2 \boldsymbol{v}} \cdot \mathbf{d}\boldsymbol{s} = -R u_n \tag{5}$$

(Note that this form is exact for a Poiseuille flow with parabolic profile). Due to separation from the outer exit, we have with outflow $\overline{v}_{\text{in}} \simeq 0$ with $\overline{v}_{\text{ex}} = u_n$ jetting out, while similarly during inflow, $\overline{v}_{\text{ex}} \simeq 0$ with $\overline{v}_{\text{in}} = u_n$ jetting into the cavity; see Fig. 2. The pressure in the jets, however, has to remain equal to the surrounding pressure (p_{ex} and p_{in} respectively) because the boundary of the jet cannot support a pressure difference. Therefore, we have altogether (redefining $\ell + 2\delta =: \ell$)

$$\rho_0 \ell \frac{\mathrm{d}}{\mathrm{d}t} u_n + \tfrac{1}{2}\rho_0 u_n |u_n| + R u_n = p_{\text{in}} - p_{\text{ex}}. \tag{6}$$

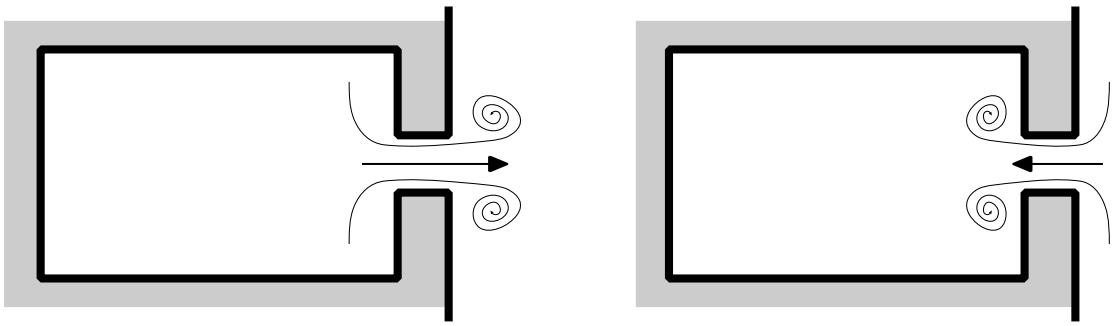

Figure 2. Separation and vortex shedding during the out-flow and in-flow phase

The second equation between p_{in} and u_n is obtained by solving the wave equation in the attached cavity (organ pipe) of uniform cross section S_b and length L, varying along $-L \leqslant x \leqslant 0$ where $x = 0$ is the position where the cavity connects to the neck. Inside the cavity, we have

$$\begin{aligned} \frac{\partial p}{\partial t} + \rho_0 c_0^2 \frac{\partial u}{\partial x} &= 0 \\ \rho_0 \frac{\partial u}{\partial t} + \frac{\partial p}{\partial x} &= 0, \end{aligned} \tag{7}$$

assuming an adiabatic compression of the fluid in the cavity $p = c_0^2 \rho$. The end conditions are then

$$\begin{aligned} u(-L, t) &= 0 \\ p(0, t) &= p_{\text{in}}(t) \\ S_b u(0, t) &= S_n u_n(t). \end{aligned} \tag{8}$$

Using d'Alembert's solution we can solve (7) to obtain

$$\begin{aligned} p(x, t) &= \rho_0 c_0^2 \big(f(c_0 t - x - L) + f(c_0 t + x + L) \big) \\ u(x, t) &= \quad c_0 \big(f(c_0 t - x - L) - f(c_0 t + x + L) \big) \end{aligned} \tag{9}$$

so

$$\begin{aligned} p_{\text{in}}(t) &= \rho_0 c_0^2 \big(f(c_0 t - L) + f(c_0 t + L) \big) \\ S_n u_n(t) &= S_b c_0 \big(f(c_0 t - L) - f(c_0 t + L) \big). \end{aligned} \tag{10}$$

After the Fourier transform of (7) using (8), we have

$$\begin{aligned} & \hat{u}(x) = A c_0 \sin(kx + kL) && \hat{p}(x) = \mathrm{i} A \rho_0 c_0^2 \cos(kx + kL), \\ \text{hence} \quad & S_n \hat{u}_n = S_b A c_0 \sin(kL) && \hat{p}_{\text{in}} = \mathrm{i} A \rho_0 c_0^2 \cos(kL). \end{aligned}$$

For the linear harmonic case, we have from (6)

$$\mathrm{i}\omega \rho_0 \ell \hat{u}_n + R \hat{u}_n = \hat{p}_{\text{in}} - \hat{p}_{\text{ex}}, \tag{11}$$

$$\hat{p}_{\text{ex}} = -\mathrm{i}\omega \rho_0 \ell \frac{S_b}{S_n} A c_0 \sin(kL) - R \frac{S_b}{S_n} A c_0 \sin(kL) + \mathrm{i} A \rho_0 c_0^2 \cos(kL). \tag{12}$$

The neck velocity $\hat{u}$ is averaged over the whole surface and can be multiplied by the porosity factor to obtain

$$\hat{u}_{\text{ex}} = \frac{S_n}{S_b} \hat{u}_n = \hat{u}(0) = A c_0 \sin(kL). \tag{13}$$

Combining (13) with (12), we obtain the standard expression of the linear impedance [16]

$$\begin{aligned} Z &= \frac{\hat{p}_{\text{ex}}}{-\hat{u}_{\text{ex}}} \\ &= \frac{-\mathrm{i}\omega \rho_0 \ell \frac{S_b}{S_n} A c_0 \sin(kL) - R \frac{S_b}{S_n} A c_0 \sin(kL) + \mathrm{i} A \rho_0 c_0^2 \cos(kL)}{A c_0 \sin(kL)} \\ &= \frac{S_b}{S_n} \big(R + \mathrm{i}\omega \rho_0 \ell \big) - \mathrm{i} \rho_0 c_0 \cot(kL). \end{aligned} \tag{14}$$

The resistance R averaged over the surface becomes the resistance term of the impedance in the linear regime. Close to resonance, the expression (14) is no longer valid because the nonlinear term in (6) is of the same order of magnitude as the other terms (the problem is formulated such that the nonlinear effects become important near resonance), as will become more clear in the next section. In order to make progress with the perturbation problem, it is essential to scale the variables in (6). This will be done in the next section.

III. Scaling

For a proper analysis, it is most clarifying to rewrite the equation into non-dimensional variables, and scaled to the right order of magnitude. For this we need an inherent timescale and pressure level. The resonance frequency ω_0 for the linearised case and $R = 0$ is evidently given by the solution of

$$\kappa_0 \tan \kappa_0 = \frac{LS_n}{\ell S_b}, \quad \kappa_0 = \frac{\omega_0 L}{c_0}. \tag{15}$$

The reciprocal of this angular frequency is a suitable timescale of the problem. By dividing the nonlinear damping term by the acceleration term we find the pressure level at which the nonlinear damping would be just as large as the other terms. So for a pressure that is a small fraction, say ε, of this level we have a problem with only little nonlinear damping. In addition we assume that the linear damping is small, and (near resonance[1]) of the same order of magnitude as the nonlinear damping. As may be expected, the driving amplitude p_{ex} will (near resonance) be an order smaller than p_{in}. In order to make all this explicit we introduce a small parameter ε (via the external forcing amplitude), and make dimensionless

$$\begin{aligned}
&\tau = \omega_0 t && p_{\text{in}}(t) = 2\varepsilon\rho_0 c_0^2 \left(\frac{\omega_0 \ell}{c_0}\right)^2 y(\tau) && p_{\text{ex}}(t) = 2\varepsilon^2 \rho_0 c_0^2 \left(\frac{\omega_0 \ell}{c_0}\right)^2 F(\tau) \\
&R = \varepsilon \rho_0 c_0 \left(\frac{\omega_0 \ell}{c_0}\right) r && u_{\text{n}}(t) = 2\varepsilon c_0 \left(\frac{\omega_0 \ell}{c_0}\right) v(\tau) && f(c_0 t) = 2\varepsilon \left(\frac{\omega_0 \ell}{c_0}\right)^2 \phi(\tau).
\end{aligned} \tag{16}$$

It should be noted that in practice the parameter R is usually a constant and not dependent of the excitation amplitude (ε). So the used scaling $\sim \varepsilon r$ should not be interpreted in that way, and is only meant to select out a certain class of problems with a relatively small linear friction and similarly small nonlinear effects. If we consider a particular configuration for varying ε but otherwise fixed, we should preserve the product εr and adapt r, but never such that r is unacceptably large and we would enter a physically different regime.

Coupled with (6) and (9), we obtain the final nonlinear differential equation

$$\frac{\mathrm{d}v}{\mathrm{d}\tau} + \varepsilon v|v| + \varepsilon r v - y = -\varepsilon F \tag{17}$$

with conditions

$$\begin{aligned}
\phi(\tau - \kappa_0) + \phi(\tau + \kappa_0) &= y(\tau) \\
\phi(\tau - \kappa_0) - \phi(\tau + \kappa_0) &= \tan \kappa_0 v(\tau)
\end{aligned} \tag{18}$$

that we need to solve asymptotically. Note that in case of small length L (the condition of [1]), we have a small κ_0, and so

$$\kappa_0 \tan \kappa_0 \sim \kappa_0^2.$$

With (15), we obtain the same resonance frequency of the cavity used by [1]. Also note that with positive ω_0, $\kappa_0 > 0$, and since the product $k_0 \tan \kappa_0 = LS_n/\ell S_b > 0$, we have $\tan \kappa_0 > 0$.

[1] Away from resonance the nonlinear effects will be much smaller.

IV. Asymptotic solution away from resonance $\omega \neq \omega_0$

Away from resonance $\omega \neq \omega_0$ and

$$F(\tau) = \cos(\Omega\tau), \quad \Omega = \frac{\omega}{\omega_0}, \tag{19}$$

our solution follows the external excitation in time, phase and order of magnitude. Hence we assume $y = O(\varepsilon)$ and expand the variables as

$$y = \varepsilon y_0 + \varepsilon^2 y_1 + \ldots, \qquad v = \varepsilon v_0 + \varepsilon^2 v_1 + \ldots, \qquad \phi = \varepsilon\phi_0 + \varepsilon^2\phi_1 + \ldots. \tag{20}$$

Collecting the like powers of ε, we obtain

$$\begin{aligned} \frac{\mathrm{d}v_0}{\mathrm{d}\tau} - y_0 &= -\cos(\Omega\tau) \\ \phi_0(\tau - \kappa_0) + \phi_0(\tau + \kappa_0) &= y_0(\tau) \\ \phi_0(\tau - \kappa_0) - \phi_0(\tau + \kappa_0) &= \tan\kappa_0 v_0(\tau) \end{aligned} \tag{21}$$

and

$$\begin{aligned} \frac{\mathrm{d}v_1}{\mathrm{d}\tau} - y_1 &= -rv_0 \\ \phi_1(\tau - \kappa_0) + \phi_1(\tau + \kappa_0) &= y_1(\tau) \\ \phi_1(\tau - \kappa_0) - \phi_1(\tau + \kappa_0) &= \tan\kappa_0 v_1(\tau). \end{aligned} \tag{22}$$

Assuming a slight amount of damping, the homogeneous solution of (21) and (22) given by appendix [A(70)] will dissipate for large time. The particular solution that remains, can be obtained as shown in appendix B. Using (73), we obtain

$$v = \varepsilon\frac{-\tan(\Omega\kappa_0)}{\Omega\tan(\Omega\kappa_0) - \tan\kappa_0}\sin(\Omega\tau) - \varepsilon^2 r\left[\frac{\tan(\Omega\kappa_0)}{\Omega\tan(\Omega\kappa_0) - \tan\kappa_0}\right]^2\cos(\Omega\tau). \tag{23}$$

which is asymptotically equivalent to the solution

$$v = -\varepsilon\tan(\Omega\kappa_0)\frac{(\Omega\tan(\Omega\kappa_0) - \tan\kappa_0)\sin(\Omega\tau) + \varepsilon r\tan(\Omega\kappa_0)\cos(\Omega\tau)}{(\Omega\tan(\Omega\kappa_0) - \tan\kappa_0)^2 + (\varepsilon r\tan(\Omega\kappa_0))^2} + O(\varepsilon^3). \tag{24}$$

We see that the response v is indeed $O(\varepsilon)$ and follows the excitation almost in phase $(\Omega\tan(\Omega\kappa_0) - \tan\kappa_0 > 0)$ or antiphase $(\Omega\tan(\Omega\kappa_0) - \tan\kappa_0 < 0)$. Close to resonance when $\Omega = 1 + O(\varepsilon)$, the term $(\Omega\tan(\Omega\kappa_0) - \tan\kappa_0) = O(\varepsilon)$, so $v = O(1)$ and the assumption that the response v has the same order as the excitation $O(\epsilon)$ is not correct. Therefore the solution (24) is not valid close to resonance.

V. Asymptotic solution close to resonance $\omega \approx \omega_0$

Near resonance, the amplitude y in (17) rises to levels of $O(1)$ with $O(\varepsilon)$ forcing and the assumption that the nonlinear damping is negligible to leading orders is not correct. As the physics of the problem essentially change when $\Omega = 1 + O(\varepsilon)$, we introduce a parameter $\sigma = O(1)$ and assume that

$$\Omega = 1 + \varepsilon\sigma. \tag{25}$$

However, posed in this form we obtain secular terms in the expansion $\cos(\tau + \varepsilon\sigma\tau) = \cos(\tau) - \varepsilon\sigma\tau\sin(\tau) + \ldots$ of the driving force, which prohibits a uniform approximation of v later [17, sec15.3.2]. Therefore, we remove the ε-dependence from the driving force by absorbing Ω into a new time coordinate $\tilde{\tau} = \Omega\tau$. Moreover, the asymptotic expansion of the term $v|v|$ introduces difficulties near the ε-dependent (and unknown) zeros of v. This will be tackled by a translation of the origin by an amount $\theta(\varepsilon)$, such that the locations of the sign change of v are fixed (as v is synchronised with the driving

force) and independent of ε. (Of course, a certain amount of smoothness is anticipated such that v has the same number of zeros per period as the forcing term). So we introduce

$$\tilde{\tau} = \Omega\tau - \theta(\varepsilon) \tag{26}$$

where θ is to be chosen such that the response v vanishes at integral multiples of π. This fixes the points along the time $\tilde{\tau}$ axis where v changes sign *i.e.*

$$v(\tilde{\tau}) = 0 \quad \text{at} \quad \tilde{\tau} = N\pi. \tag{27}$$

In other words, $\Omega\tau = \omega t = \theta$ corresponds with the phase lag of response v_{ex} to excitation p_{ex} like in [1]. Consider $\Omega = 1 + O(\varepsilon)$ and introduce the transformation

$$F = F_0\cos(\tilde{\tau}+\theta),\ \Omega = 1+\varepsilon\sigma,\ \tilde{\tau} = \Omega\tau - \theta,\ y(\tau) = \tilde{y}(\tilde{\tau}),\ v(\tau) = \tilde{v}(\tilde{\tau}) \text{ and } \phi(\tau) = \tilde{\phi}(\tilde{\tau}), \tag{28}$$

to obtain the following set of equations

$$\Omega\frac{\mathrm{d}\tilde{v}}{\mathrm{d}\tilde{\tau}} + \varepsilon\tilde{v}|\tilde{v}| + \varepsilon r\tilde{v} - \tilde{y} = -\varepsilon F \tag{29}$$

with

$$\begin{aligned} \tilde{\phi}(\tilde{\tau} - \Omega\kappa_0) + \tilde{\phi}(\tilde{\tau} + \Omega\kappa_0) &= \tilde{y}(\tilde{\tau}) \\ \tilde{\phi}(\tilde{\tau} - \Omega\kappa_0) - \tilde{\phi}(\tilde{\tau} + \Omega\kappa_0) &= \tan\kappa_0\tilde{v}(\tilde{\tau}). \end{aligned} \tag{30}$$

Now we expand the variables as follows

$$\begin{aligned} &\tilde{y} = \tilde{y}_0 + \varepsilon\tilde{y}_1 + \ldots, \quad \tilde{v} = \tilde{v}_0 + \varepsilon\tilde{v}_1 + \ldots, \quad \tilde{\phi} = \tilde{\phi}_0 + \varepsilon\tilde{\phi}_1 + \ldots, \quad \theta = \theta_0 + \varepsilon\theta_1 + \ldots, \\ &\tilde{\phi}(\tilde{\tau} \pm \Omega\kappa_0) = \tilde{\phi}_0(\tilde{\tau} \pm \kappa_0) + \varepsilon\big(\tilde{\phi}_1(\tilde{\tau} \pm \kappa_0) \pm \sigma\kappa_0\tilde{\phi}_0'(\tilde{\tau} \pm \kappa_0)\big) \\ &\qquad\qquad + \varepsilon^2\left[\tilde{\phi}_2(\tilde{\tau} \pm \kappa_0) + \tfrac{1}{2}(\sigma\kappa_0)^2\tilde{\phi}_0''(\tilde{\tau} \pm \kappa_0) \pm \sigma\kappa_0\tilde{\phi}_1'(\tilde{\tau} \pm \kappa_0) + \right] + \ldots. \end{aligned} \tag{31}$$

Next we collect the terms of the same order of ε and construct our solution in the form of an asymptotic series.

Order ε^0 analysis:

Substituting (31) in (30) and afterwards in (29) and collecting the terms of $O(\varepsilon^0)$, we have

$$\begin{aligned} \frac{\mathrm{d}\tilde{v}_0}{\mathrm{d}\tilde{\tau}} - \tilde{y}_0 &= 0 \\ \tilde{\phi}_0(\tilde{\tau} - \kappa_0) + \tilde{\phi}_0(\tilde{\tau} + \kappa_0) &= \tilde{y}_0(\tilde{\tau}) \\ \tilde{\phi}_0(\tilde{\tau} - \kappa_0) - \tilde{\phi}_0(\tilde{\tau} + \kappa_0) &= \tan\kappa_0\tilde{v}_0(\tilde{\tau}). \end{aligned} \tag{32}$$

At large times, assuming a little damping, the cavity is driven by the external force in such a way that a steady state is reached and the initial conditions are not important. Hence from (70), we choose the steady solution and obtain, using (27),

$$\tilde{\phi}_0 = \tfrac{1}{2}A_0\cos\tilde{\tau}, \tag{33}$$

and hence

$$\tilde{y}_0 = A_0\cos\kappa_0\cos\tilde{\tau} \quad \text{and} \quad \tilde{v}_0 = A_0\cos\kappa_0\sin\tilde{\tau}, \tag{34}$$

where A_0 and θ_0 are to be determined from the regularity condition (absence of secular terms (74)) in the next order ε^1.

Order ε^1 analysis:

Collecting the terms of $O(\varepsilon)$ from (29), we obtain

$$\begin{aligned}
\frac{\mathrm{d}\tilde{v}_1}{\mathrm{d}\tilde{\tau}} - \tilde{y}_1 &= -\sigma\tilde{v}_0' - \tilde{v}_0|\tilde{v}_0| - r\tilde{v}_0 - F_0\cos(\tilde{\tau}+\theta_0) \\
\tilde{\phi}_1(\tilde{\tau}-\kappa_0) + \tilde{\phi}_1(\tilde{\tau}+\kappa_0) &= \sigma\kappa_0\tilde{\phi}_0'(\tilde{\tau}-\kappa_0) - \sigma\kappa_0\tilde{\phi}_0'(\tilde{\tau}+\kappa_0) + \tilde{y}_1(\tilde{\tau}) \\
\tilde{\phi}_1(\tilde{\tau}-\kappa_0) - \tilde{\phi}_1(\tilde{\tau}+\kappa_0) &= \sigma\kappa_0\tilde{\phi}_0'(\tilde{\tau}-\kappa_0) + \sigma\kappa_0\tilde{\phi}_0'(\tilde{\tau}+\kappa_0) + \tan\kappa_0\tilde{v}_1(\tilde{\tau}).
\end{aligned} \tag{35}$$

From (33), (34) and (35), we have after eliminating $\tilde{y}_1$ and $\tilde{v}_1$

$$\begin{aligned}
&\frac{1}{\tan\kappa_0}\left[\tilde{\phi}_1'(\tilde{\tau}-\kappa_0) - \tilde{\phi}_1'(\tilde{\tau}+\kappa_0)\right] - \left[\tilde{\phi}_1(\tilde{\tau}-\kappa_0) + \tilde{\phi}_1(\tilde{\tau}+\kappa_0)\right] = \\
&\quad -\sigma\frac{\kappa_0}{\tan\kappa_0}A_0\cos\kappa_0\cos\tilde{\tau} + \sigma\kappa_0 A_0\sin\kappa_0\cos\tilde{\tau} - \sigma A_0\cos\kappa_0\cos\tilde{\tau} \\
&\qquad - A_0|A_0|\cos^2\kappa_0\sin\tilde{\tau}|\sin\tilde{\tau}| - rA_0\cos\kappa_0\sin\tilde{\tau} - F_0\cos\tilde{\tau}\cos\theta_0 + F_0\sin\tilde{\tau}\sin\theta_0.
\end{aligned} \tag{36}$$

From the arguments that we just have the stationary solution and its asymptotic expansion is uniform in $\tilde{\tau}$, it follows that no resonant excitation is allowed in the right hand side of the equation (36). This means (see (74)) that we should suppress the cos- and sin-terms including those in the Fourier expansion of

$$\sin(x)|\sin(x)| \sim \frac{8}{3\pi}\sin(x) - \frac{8}{15\pi}\sin(3x) - \ldots.$$

Hence we obtain the algebraic equations

$$\begin{aligned}
F_0\cos\theta_0 &= -\sigma A_0\left[\frac{\kappa_0}{\tan\kappa_0}\cos\kappa_0 + \cos\kappa_0 - \kappa_0\sin\kappa_0\right] \\
F_0\sin\theta_0 &= \quad A_0\left[\frac{8}{3\pi}\cos^2\kappa_0|A_0| + r\cos\kappa_0\right].
\end{aligned} \tag{37}$$

In general, A_0 has to be solved numerically, from which θ_0 follows. There exist two (real) solutions, while if (A_0, θ_0) is a solution, then also $(-A_0, \theta_0+\pi)$. So, if convenient, we could assume that A_0 is positive and maintain $|A_0| = A_0$, but this depends on θ_0. Solving (37), we can obtain A_0 and θ_0 as plotted in Fig. 3. We notice that the amplitude rises to $O(1)$ at resonance and decays when $\sigma \to \pm\infty$.

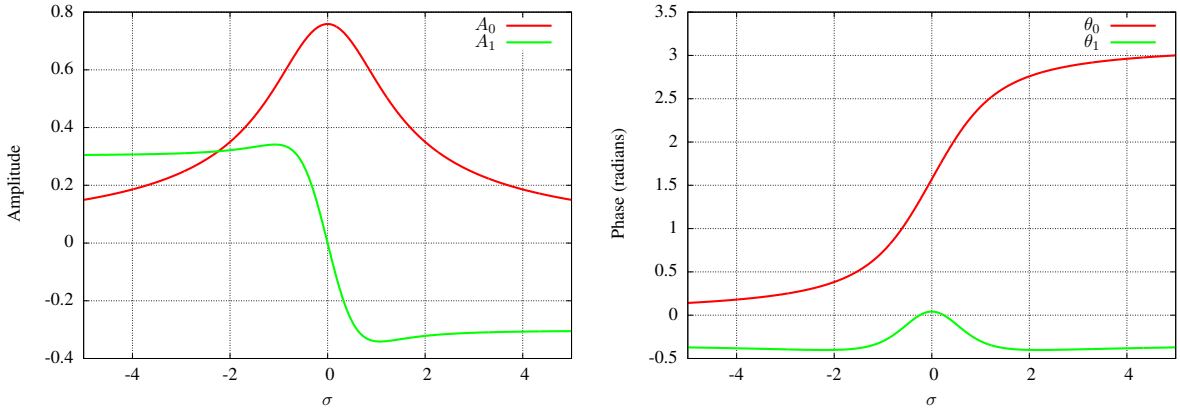

Figure 3. Solution of amplitude (A_0, A_1) and phase (θ_0, θ_1) as a function of σ, with $\kappa_0 = 0.55$, and $r = F_0 = 1$

If we take the low frequency limit ($\kappa_0 \to 0$) in (37), we obtain exactly the same equations as in [1]. Physically, in this limit, the cavity length L would be asymptotically smaller than the acoustic wavelength $2\pi c_0/\omega_0$ and hence the wave would feel a uniform pressure inside the cavity and thus the current modelling assumption converges to the one in [1].

From (36), we have

$$\frac{1}{\tan\kappa_0}\left[\tilde{\phi}_1'(\tilde{\tau}-\kappa_0)-\tilde{\phi}_1'(\tilde{\tau}+\kappa_0)\right]-\left[\tilde{\phi}_1(\tilde{\tau}-\kappa_0)+\tilde{\phi}_1(\tilde{\tau}+\kappa_0)\right] = \frac{A_0^2\cos^2(\kappa_0)}{\pi}\sum_{n=1}^{\infty}\frac{\sin(2n+1)\tilde{\tau}}{(n^2-\frac{1}{4})(n+\frac{3}{2})}$$

which can be solved term-wise using (70), similar to (33), to obtain

$$\tilde{\phi}_1(\tilde{\tau}) = \tfrac{1}{2}A_1\cos\tilde{\tau}+\tfrac{1}{2}B_1\sin\tilde{\tau} + \frac{A_0^2\cos^2\kappa_0\tan\kappa_0}{2\pi}\sum_{n=1}^{\infty}\frac{\sin(2n+1)\tilde{\tau}}{\cos((2n+1)\kappa_0)\left[(2n+1)\tan((2n+1)\kappa_0)-\tan\kappa_0\right](n^2-\frac{1}{4})(n+\frac{3}{2})} \tag{38}$$

which upon substituting in (35) gives

$$\tilde{v}_1(\tilde{\tau}) = A_1\cos\kappa_0\sin\tilde{\tau}-B_1\cos\kappa_0\cos\tilde{\tau}+\sigma\kappa_0 A_0\frac{\cos\kappa_0}{\tan\kappa_0}\sin\tilde{\tau} - \frac{A_0^2\cos^2\kappa_0}{\pi}\sum_{n=1}^{\infty}\frac{\cos(2n+1)\tilde{\tau}}{\left[(2n+1)-\frac{\tan\kappa_0}{\tan((2n+1)\kappa_0)}\right](n^2-\frac{1}{4})(n+\frac{3}{2})}. \tag{39}$$

Using the condition (27), *i.e.* $\tilde{v}_1(\tilde{\tau}=N\pi)=0$, we find

$$B_1 = -\frac{A_0^2\cos^2\kappa_0}{\pi}\sum_{n=1}^{\infty}\frac{1}{\left[(2n+1)-\frac{\tan\kappa_0}{\tan((2n+1)\kappa_0)}\right](n^2-\frac{1}{4})(n+\frac{3}{2})}. \tag{40}$$

Note that in the limit $\kappa_0\to 0$, we have $B_1=-\frac{2}{9\pi}A_0^2$, which is useful for later. The other two unknowns A_1 and θ_1 are to be determined from the regularity condition at next order (ε^2).

Order ε^2 analysis:

Collecting the terms of $O(\varepsilon^2)$ from (29), we obtain

$$\begin{aligned}
\tilde{v}_2'-\tilde{y}_2 &= -\sigma\tilde{v}_1'-2\tilde{v}_1|\tilde{v}_0|-r\tilde{v}_1+\theta_1\sin(\tilde{\tau}+\theta_0)\\
\tilde{\phi}_2(\tilde{\tau}-\kappa_0)+\tilde{\phi}_2(\tilde{\tau}+\kappa_0) &= -\tfrac{1}{2}(\sigma\kappa_0)^2\left[\tilde{\phi}_0''(\tilde{\tau}-\kappa_0)+\tilde{\phi}_0''(\tilde{\tau}+\kappa_0)\right]\\
&\quad +\sigma\kappa_0\left[\tilde{\phi}_1'(\tilde{\tau}-\kappa_0)-\tilde{\phi}_1'(\tilde{\tau}+\kappa_0)\right]+\tilde{y}_2(\tilde{\tau})\\
\tilde{\phi}_2(\tilde{\tau}-\kappa_0)-\tilde{\phi}_2(\tilde{\tau}+\kappa_0) &= -\tfrac{1}{2}(\sigma\kappa_0)^2\left[\tilde{\phi}_0''(\tilde{\tau}-\kappa_0)-\tilde{\phi}_0''(\tilde{\tau}+\kappa_0)\right]\\
&\quad +\sigma\kappa_0\left[\tilde{\phi}_1'(\tilde{\tau}-\kappa_0)+\tilde{\phi}_1'(\tilde{\tau}+\kappa_0)\right]+\tan\kappa_0\tilde{v}_2(\tilde{\tau}).
\end{aligned} \tag{41}$$

Substituting $\tilde{y}_2$ and $\tilde{v}_2$ in the first equation of (41), we obtain

$$\begin{aligned}
&\frac{1}{\tan\kappa_0}\left[\tilde{\phi}_2'(\tilde{\tau}-\kappa_0)-\tilde{\phi}_2'(\tilde{\tau}+\kappa_0)\right]-\left[\tilde{\phi}_2(\tilde{\tau}-\kappa_0)+\tilde{\phi}_2(\tilde{\tau}+\kappa_0)\right]=\\
&\tfrac{1}{2}(\sigma\kappa_0)^2\left[\tilde{\phi}_0''(\tilde{\tau}-\kappa_0)+\tilde{\phi}_0''(\tilde{\tau}+\kappa_0)\right]-\frac{(\sigma\kappa_0)^2}{2\tan\kappa_0}\left[\tilde{\phi}_0'''(\tilde{\tau}-\kappa_0)-\tilde{\phi}_0'''(\tilde{\tau}+\kappa_0)\right]\\
&\quad -\sigma\kappa_0\left[\tilde{\phi}_1'(\tilde{\tau}-\kappa_0)-\tilde{\phi}_1'(\tilde{\tau}+\kappa_0)\right]+\frac{\sigma\kappa_0}{\tan\kappa_0}\left[\tilde{\phi}_1''(\tilde{\tau}-\kappa_0)+\tilde{\phi}_1''(\tilde{\tau}+\kappa_0)\right]\\
&\quad -\sigma\tilde{v}_1'-2\tilde{v}_1|\tilde{v}_0|-r\tilde{v}_1+\theta_1\sin(\tilde{\tau}+\theta_0),
\end{aligned} \tag{42}$$

in which we have to suppress the sine - cosine terms to obtain A_1 and θ_1.

Using (33), (34), (38), (39) and (40) with (42), (see appendix [C]) and collecting the coefficients of cosine and sine terms and equating them to zero, we obtain a set of 2 linear equations with variables A_1 and θ_1

$$\begin{aligned}\left[\sigma\kappa_0\sin\kappa_0+\frac{\sigma\kappa_0}{\tan\kappa_0}\cos\kappa_0+\sigma\cos\kappa_0\right]A_1-\theta_1\sin\theta_0=\\ \left(r\cos\kappa_0+\frac{8}{3\pi}A_0\cos^2\kappa_0\right)B_1-\sigma^2\kappa_0\frac{\cos\kappa_0}{\tan\kappa_0}A_0\\ -\frac{2A_0^3\cos^3\kappa_0}{\pi^2}\sum_{n=1}^{\infty}\frac{1}{\left[(2n+1)-\frac{\tan\kappa_0}{\tan((2n+1)\kappa_0)}\right](n^2-\frac{1}{4})(n+\frac{3}{2})(n-\frac{1}{2})(n+\frac{3}{2})}\end{aligned}\tag{43}$$

$$\begin{aligned}\left[r\cos\kappa_0+\frac{16}{3\pi}A_0\cos^2\kappa_0\right]A_1-\theta_1\cos\theta_0=\\ -\left(\sigma\kappa_0\sin\kappa_0+\frac{\sigma\kappa_0}{\tan\kappa_0}\cos\kappa_0+\sigma\cos\kappa_0\right)B_1-r\sigma\kappa_0\frac{\cos\kappa_0}{\tan\kappa_0}A_0-\frac{16}{3\pi}\sigma\kappa_0\frac{\cos^2\kappa_0}{\tan\kappa_0}A_0^2.\end{aligned}$$

Solving (43), we can determine A_1 and θ_1 as shown in Fig. 3. Hence we have the solution correct till $O(\varepsilon)$. In the limit $\kappa_0\to 0$ and noting that $\sum_{n=1}^{\infty}\frac{(2n+1)}{4n(n+1)(n^2-\frac{1}{4})(n+\frac{3}{2})^2(n-\frac{1}{2})}=\frac{9\pi^2-80}{54}$, we obtain from (43)

$$\begin{aligned}2\sigma A_1-\theta_1\sin\theta_0&=-\sigma^2A_0-\left[\frac{1}{3}-\frac{64}{27\pi^2}\right]A_0^3-\frac{2}{9\pi}rA_0^2\\ \left[\frac{16}{3\pi}A_0+r\right]A_1-\theta_1\cos\theta_0&=-r\sigma A_0-\frac{44}{9\pi}\sigma A_0^2\end{aligned}\tag{44}$$

which is exactly the equation set of [1], as expected. This confirms the consistency of the current and previous solutions. Using (39), (31), (28) and (16), we finally obtain

$$\begin{aligned}u_n=&2\varepsilon\ell\omega_0\left[(A_0\cos\kappa_0+\varepsilon A_1\cos\kappa_0+\varepsilon\sigma\kappa_0A_0\frac{\cos\kappa_0}{\tan\kappa_0})\sin(\omega t-\theta)-\varepsilon B_1\cos\kappa_0\cos(\omega t-\theta)\right]\\ &-2\varepsilon^2\ell\omega_0\frac{A_0^2\cos^2\kappa_0}{\pi}\sum_{n=1}^{\infty}\frac{\cos(2n+1)(\omega t-\theta)}{\left[(2n+1)-\frac{\tan\kappa_0}{\tan((2n+1)\kappa_0)}\right](n^2-\frac{1}{4})(n+\frac{3}{2})}.\end{aligned}\tag{45}$$

The velocity in (45) after averaging over the surface (multiplying with S_n/S_b) can be used with the external excitation in (16) to obtain the impedance that we will derive in the next section. It is interesting to note that, to the leading orders,

$$u_n(t)=2\varepsilon\ell\omega_0A_0\cos\kappa_0\sin(\omega t-\theta_0).\tag{46}$$

If we expand the function $\tilde{\phi}(\tilde{\tau}-\Omega\kappa_0)$ about $\Omega\kappa_0$ in (30) assuming small κ_0, we obtain

$$\tilde{y}(\tilde{\tau})=2\tilde{\phi}(\tilde{\tau})\qquad\text{and}\qquad\tilde{v}(\tilde{\tau})=-2\Omega\tilde{\phi}'(\tilde{\tau}),\tag{47}$$

that can be substituted back in (29) to obtain

$$\Omega^2\tilde{y}''(\tilde{\tau})+\varepsilon\Omega^2\tilde{y}'(\tilde{\tau})|\tilde{y}'(\tilde{\tau})|+\varepsilon\Omega r\tilde{y}'(\tilde{\tau})+\tilde{y}(\tilde{\tau})=\varepsilon F\tag{48}$$

which is exactly the equation analysed by [1] in the nonlinear regime with the condition that the pressure inside the cavity is uniform and the velocity inside is given by the time derivative of pressure $i.e.$

$$V\frac{\mathrm{d}p_{\text{in}}}{\mathrm{d}t}=-\rho_0c_0^2u_nS_n\tag{49}$$

where $V=S_bL$ is the volume of the cavity. From (34) and (16), we obtain

$$p_{\text{in}}(t)=2\varepsilon\rho_0\ell^2\omega_0^2A_0\cos(\omega t-\theta_0)\tag{50}$$

which upon substituting in (49) gives

$$u_n(t) = 2\varepsilon\omega\ell A_0 \sin(\omega t - \theta_0). \tag{51}$$

The neck velocity $u_n(t)$ in (51) is exactly the one obtained by [1] with the term ω instead of ω_0 like in (45). Note that close to resonance $\Omega = \omega/\omega_0 \approx 1$, ω and ω_0 are asymptotically equivalent. However, the two different approaches of cavity modelling produce different, but asymptotically equivalent form of solutions.

VI. Impedance calculation

In order to obtain realistic numbers, we will consider the impedance Z as the effective impedance of an array of Helmholtz resonators, where the spatially averaged neck velocity is identified to the external acoustic velocity. Therefore, we add a porosity factor S_n/S_b to u_n and obtain

$$v_{\text{ex}} = \frac{S_n}{S_b} u_n. \tag{52}$$

Then we define the impedance as the ratio of the Fourier transforms of the external pressure p_{ex} and (minus) the external velocity v_{ex} at excitation frequency ω.

$$Z(\eta) = \frac{\hat{p}_{\text{ex}}(\eta)}{-\hat{v}_{\text{ex}}(\eta)} = \frac{\dfrac{1}{2\pi}\displaystyle\int_{-\infty}^{\infty} p_{\text{ex}}(t)\,\mathrm{e}^{-\mathrm{i}\eta t}\,\mathrm{d}t}{-\dfrac{1}{2\pi}\displaystyle\int_{-\infty}^{\infty} v_{\text{ex}}(t)\,\mathrm{e}^{-\mathrm{i}\eta t}\,\mathrm{d}t} \quad (\eta = \omega). \tag{53}$$

VI.A. Non-resonant impedance

Taking the Fourier transformation of $p_{\text{ex}}(t)$ from (16) and Fourier transformation of $v_{\text{ex}}(t) = (S_n/S_b)u_{\text{n}}(t)$ from (24), we obtain for $\eta > 0$,

$$\begin{aligned}
\hat{p}_{\text{ex}}(\eta) =& \frac{1}{2\pi}\int_{-\infty}^{\infty} p_{\text{ex}}(t)\,\mathrm{e}^{-\mathrm{i}\eta t}\,\mathrm{d}t = \frac{1}{2\pi}\varepsilon^2\rho_0\ell^2\omega_0^2\,F_0\delta(\eta-\omega)\\
\hat{v}_{\text{ex}}(\eta) =& \frac{1}{2\pi}\int_{-\infty}^{\infty} v_{\text{ex}}(t)\,\mathrm{e}^{-\mathrm{i}\eta t}\,\mathrm{d}t\\
=& \frac{1}{2\pi}\frac{S_n}{S_b}\varepsilon^2\omega_0\ell\left[\frac{-\tan(\Omega\kappa_0)}{\Omega\tan(\Omega\kappa_0)-\tan\kappa_0}\frac{1}{\mathrm{i}} - \varepsilon r\left(\frac{\tan(\Omega\kappa_0)}{\Omega\tan(\Omega\kappa_0)-\tan\kappa_0}\right)^2\right]\delta(\eta-\omega)
\end{aligned} \tag{54}$$

with the negative of the ratio of above two in (54) being the impedance, given by

$$Z(\omega) = \frac{S_b}{S_n}\rho_0\ell\omega_0\left[\frac{\tan(\Omega\kappa_0)}{\Omega\tan(\Omega\kappa_0)-\tan\kappa_0}\frac{1}{\mathrm{i}} + \varepsilon r\left(\frac{\tan(\Omega\kappa_0)}{\Omega\tan(\Omega\kappa_0)-\tan\kappa_0}\right)^2\right]^{-1}. \tag{55}$$

To leading orders in ε, the impedance expression in (55) indeed becomes the one in (14) as expected.

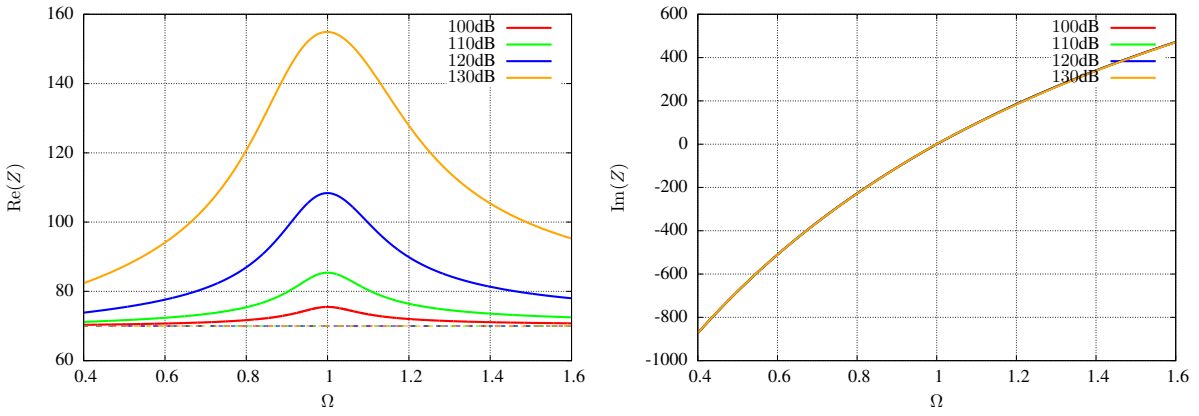

p_{ex} (dB)	100	110	120	130
ε	0.0337	0.0599	0.1065	0.1893

Figure 4. Real and imaginary parts of impedance Z for an extended Helmholtz resonator as a function of nondimensional frequency at different driving amplitudes. The realistic configuration that is chosen corresponds with $\ell = 0.005$ m, $L = 0.035$ m and $S_n/S_b = 0.05$ that gives $\kappa_0 = 0.55$ and $\omega_0 = 5367$ rad/sec, while $F_0 = 1$. The dashed line represents the linear resistance[3] which is obtained by multiplying $R = 3.5$ with porosity factor *i.e.* $(S_b/S_n)R = 70$.

VI.B. Resonant impedance

Taking the Fourier transformation of p_{ex} from (16) and Fourier transformation of $v_{\text{ex}}(t) = (S_n/S_b)u_{\text{n}}(t)$ from (45), we have for $\eta > 0$

$$\hat{p}_{\text{ex}}(\eta) = \frac{1}{2\pi}\int_{-\infty}^{\infty} p_{\text{ex}}(t)\,\mathrm{e}^{-\mathrm{i}\eta t}\,\mathrm{d}t = \frac{1}{2\pi}\varepsilon^2\rho_0\ell^2\omega_0^2\,F_0\delta(\eta-\omega), \tag{56}$$

$$\begin{aligned}\hat{v}_{\text{ex}}(\eta) &= \frac{1}{2\pi}\int_{-\infty}^{\infty} v_{\text{ex}}(t)\,\mathrm{e}^{-\mathrm{i}\eta t}\,\mathrm{d}t \\ &= \frac{-\mathrm{i}}{2\pi}\frac{S_n}{S_b}\varepsilon\omega_0\ell\,\mathrm{e}^{-\mathrm{i}\theta}\left[A_0\cos\kappa_0 + \varepsilon A_1\cos\kappa_0 + \varepsilon\sigma\kappa_0 A_0\frac{\cos\kappa_0}{\tan\kappa_0} - \mathrm{i}\varepsilon B_1\cos\kappa_0\right]\delta(\eta-\omega).\end{aligned} \tag{57}$$

Substituting (56) and (57) in (53), we obtain

$$Z(\omega) = \varepsilon\rho_0\ell\omega_0\frac{S_b}{S_n}\frac{-\mathrm{i}\,\mathrm{e}^{\mathrm{i}\theta}\,F_0}{A_0\cos\kappa_0 + \varepsilon(A_1\cos\kappa_0 + \sigma A_0\cos\kappa_0\frac{\kappa_0}{\tan\kappa_0} - \mathrm{i}B_1\cos\kappa_0)}. \tag{58}$$

In order to illustrate formula (58), we have plotted in Fig. 4 resistance $\mathrm{Re}(Z)$ and reactance $\mathrm{Im}(Z)$ as a function of Ω, obtained for a typical geometry at different driving amplitudes, corresponding with ε varying from 0.03 to 0.19. As may be expected from (58), the main effect of the forcing amplitude is in the resistance. The reactance is practically independent of it. Typically, the resistance increases everywhere with the amplitude, being highest at or near the resonance frequency and decaying along both sides, but more for frequencies less than the resonance frequency. Away from the resonance, if we take the limit $\sigma \to \pm\infty$, in (58), we obtain the linear impedance described by (14). Hence, the nonlinear impedance matches asymptotically to the linear impedance which confirms the consistency of our nonlinear solution.

VI.B.1. Effect of second order approximation and organ pipe cavity on the resistance

In order to understand the effect of the second order approximation on the resistance, the resistances obtained from the first ($\tilde{v}_0$) and second ($\tilde{v}_0 + \varepsilon\tilde{v}_1$) order approximations are shown in Fig. 5 (*left*). As

[3]Note: r is adapted such that εr is kept fixed.

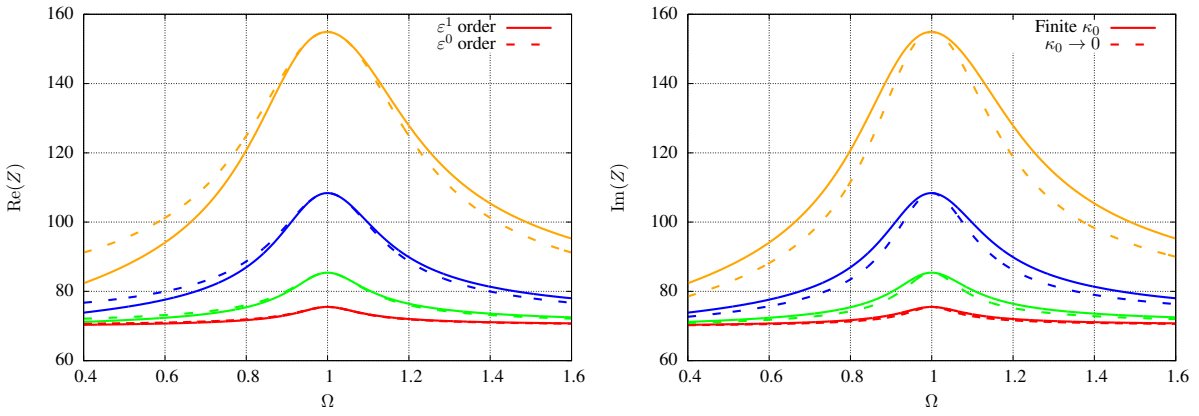

Figure 5. Resistance, $\mathrm{Re}(Z)$ as a function of nondimensional frequency at different driving amplitudes. The configuration of the resonator and deriving amplitudes are the same as in Fig. 4.

we can see, for lower driving amplitudes, the second order correction is not necessary. It is, however, essential for higher amplitudes.

In order to understand the effect of the organ pipe type cavity on the resistance term, we take the limit $\kappa_0 \to 0$ in (58) and obtain the expression

$$\begin{aligned} Z(\omega) &\sim \varepsilon\rho_0\ell\omega_0 \frac{S_b}{S_n} \frac{-\mathrm{i}\,\mathrm{e}^{\mathrm{i}\theta} F_0}{(A_0 + \varepsilon A_1 + \varepsilon\sigma A_0 + \mathrm{i}\varepsilon\frac{2}{9\pi}A_0^2)} \\ &= \frac{\varepsilon\rho_0 c_0^2 F_0}{L\omega_0} \frac{-\mathrm{i}\,\mathrm{e}^{\mathrm{i}\theta}}{A_0(1+\varepsilon\sigma) + \mathrm{i}\varepsilon\frac{2}{9\pi}A_0^2 + \varepsilon A_1}. \end{aligned} \tag{59}$$

The plots of resistance obtained with finite κ_0 (58) and $\kappa_0 \to 0$ (59) are shown in Fig. 5 *(right)*. For very low amplitudes, this effect is minor, but it is quite essential for higher amplitudes. Also, we notice that a finite κ_0 resistance curve has a better behavior away from the resonance frequency when compared with the experimental data curve in Fig. 7 *(right)*.

VI.B.2. Comparison with previous model [1]

The impedance expression found by [1],

$$\begin{aligned} Z(\omega) &= \frac{\varepsilon\rho_0 c_0^2 F_0}{L\omega} \frac{-\mathrm{i}\,\mathrm{e}^{\mathrm{i}\theta}}{A_0 + \mathrm{i}\varepsilon\frac{2}{9\pi}A_0^2 + \varepsilon A_1} \\ &= \frac{\varepsilon\rho_0 c_0^2 F_0}{L\omega_0} \frac{-\mathrm{i}\,\mathrm{e}^{\mathrm{i}\theta}}{A_0(1+\varepsilon\sigma) + \mathrm{i}\varepsilon\frac{2}{9\pi}A_0^2 + \varepsilon A_1 + \varepsilon\sigma(\mathrm{i}\varepsilon\frac{2}{9\pi}A_0^2 + \varepsilon A_1)}, \end{aligned} \tag{60}$$

is asymptotically equivalent, up to $O(\varepsilon^2)$, to (59). Shown in Fig. 6 is the plot of the resistance obtained from (60), (58) and (59), for a typical geometry and external excitation, varying from 100dB to 130dB and the resistance factor $r = 1$. The current model with finite κ_0 (58) indeed predicts the near resonance behavior to a better accuracy and decays away from the resonance to match with the linear resistance. The resistance predicted by (59) follows the same. The near resonance behaviour of [1] is similar to previous ones, however, with higher ε and away from the resonance, the resistance does not decay. It turns out just by sheer luck that (59), although asymptotically equivalent to (60), gives far better predictions at finite ε. Hence, as a concluding remark, we suggest to use the asymptotically equivalent form (59) as the impedance expression derived in [1].

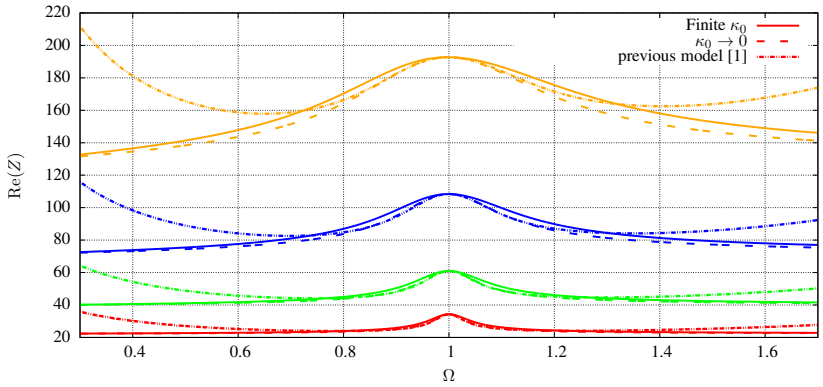

Figure 6. Comparison of resistance, $\mathrm{Re}(Z)$ based upon the current model and [1] as a function of nondimensional frequency at different driving amplitudes. The configuration of the resonator and deriving amplitudes are the same as in Fig. 4, except that $r = 1$ is kept constant.

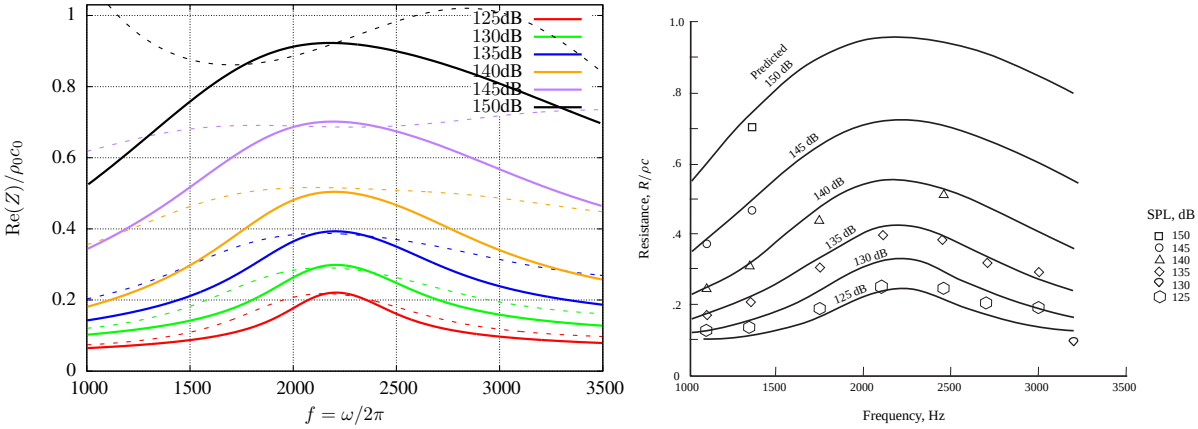

p_{ex} (dB)	125	130	135	140	145	150
ε	0.1373	0.1830	0.2441	0.3255	0.4340	0.5788

Figure 7. Comparison of (58) with measurements and predictions of $\mathrm{Re}(Z)/\rho_0 c_0$ given in [7]. The solid lines in the left corresponds to the resistance values produced by (58) while the dotted lines corresponds to the previous model [1]. The markers in the right figure represent the measured values which were used, by adopting the relation $R = \rho_0 c_0(a + b|v|)$, to predict the resistance in solid curves.

VII. Comparison with Motsinger and Craft [7]

The behavior in (58) may be compared in Fig. 7 with the measurements and predictions given by Motsinger and Kraft in [7]. Their predictions are (a.o.) based on a resistance of the form $R = \rho_0 c_0(a + b|v|)$ with suitably chosen a and b. The parameter values we used are based on $\omega_0/2\pi = 2209.1\,\mathrm{Hz}$, $\ell = 0.002\,\mathrm{m}$, $L = 0.014\,\mathrm{m}$, $S_n/S_b = 0.05$ and $\kappa_0 = 0.5715$. The resistance term $R = 1.7$, so the linear resistance $(S_b/S_n)R = 34$, divided by $\rho_0 c_0$, to have the linear level at about 0.08 in Fig. 7. Unfortunately, only little experimental data for the higher amplitudes are available. However, the agreement is remarkably good, even when ε is relatively large for higher amplitudes. The impedance for higher amplitude (ε) at and near resonance is predicted much more accurately compared to the previous model, which is plotted by dotted lines. So we conclude that the current model has indeed a better accuracy and could be used to predict the impedance for resonators of small or big lengths.

VIII. Conclusions

A systematic approximation of the hydrodynamically nonlinear Helmholtz resonator equation that includes higher order axial modes in the cavity is obtained, including the resulting impedance if the resonator as applied in an acoustic liner. The only unknown parameter that we need to adapt is resistance factor r, and sometimes the effective neck length ℓ is also unknown and has to be estimated. Com-

parisons with measurements show that the model predicts the near resonance impedance behaviour at $\sigma = O(1)$ to a good accuracy and a better resemblance is found (especially for higher excitation amplitudes) compared to the previous model [1]. The real part of the found impedance (the resistance) shows the usual characteristic behavior as a function of frequency, namely a maximum at the resonance frequency and a decay along both sides. All values increase with the amplitude. The imaginary part of the impedance (the reactance) is linear in frequency in a way that it vanishes at resonance and is practically independent of the amplitude. The nonlinear solution asymptotically matches smoothly with the linear solution, which confirms the consistency of our solution.

Acknowledgement

We gratefully acknowledge the support from the European Union through ITN-project *FlowAirS* (contract no. FP7-PEOPLE-2011-ITN-289352), with coordinator Yves Aurégan.

Appendix

A. Solution of homogeneous problem

Consider the homogeneous equation

$$\begin{aligned} \frac{\mathrm{d}v}{\mathrm{d}\tau} - y &= 0 \\ \phi(\tau-\kappa_0) + \phi(\tau+\kappa_0) &= y(\tau) \\ \phi(\tau-\kappa_0) - \phi(\tau+\kappa_0) &= \tan\kappa_0 v(\tau). \end{aligned} \tag{61}$$

Assume for the homogeneous problem the trial solutions

$$y = A\,\mathrm{e}^{\mathrm{i}\lambda\tau}, \quad v = B\,\mathrm{e}^{\mathrm{i}\lambda\tau}, \quad \phi = C\,\mathrm{e}^{\mathrm{i}\lambda\tau}\,. \tag{62}$$

Substituting (62) back into (61), we find

$$2C\cos(\lambda\kappa_0) = A = \mathrm{i}\lambda B, \quad -2\mathrm{i}C\sin(\lambda\kappa_0) = \tan\kappa_0 B, \tag{63}$$

leading to

$$\lambda\tan(\lambda\kappa_0) = \tan\kappa_0. \tag{64}$$

All solutions of (64) come in pairs. If λ is solution then $-\lambda$ is also a solution. However from (15), we notice that for a positive ω_0, $\kappa_0 >$ and since product $\kappa_0\tan\kappa_0 = LS_n/\ell S_b$ is a positive constant, $\tan\kappa_0 < 0$ does not occur. For $\tan\kappa_0 > 0$, λ is given as

$$\lambda_1 = 1, \quad \lambda_2, \quad \lambda_3, \ldots. \tag{65}$$

For example: if $\kappa_0 = \frac{1}{4}\pi$ and $\tan\kappa_0 = 1$, then

$$\lambda_1 = 1, \quad \lambda_2 = 4.291488, \quad \lambda_3 = 8.1553478 \quad \text{etc.} \tag{66}$$

So the general solution for $\tan\kappa_0 > 0$ is[4]

$$y = a_1\cos\tau + b_1\sin\tau + \sum_{n=2}^{\infty} a_n\cos(\lambda_n\tau) + b_n\sin(\lambda_n\tau). \tag{70}$$

B. Solution of inhomogeneous problem

Assume for the inhomogeneous problem

$$\begin{aligned} \frac{\mathrm{d}v}{\mathrm{d}\tau} &= y + \mathrm{e}^{\mathrm{i}\Omega\tau} \\ \phi(\tau-\kappa_0) + \phi(\tau+\kappa_0) &= y(\tau) \\ \phi(\tau-\kappa_0) - \phi(\tau+\kappa_0) &= \tan\kappa_0 v(\tau), \end{aligned} \tag{71}$$

[4]Although it is not relevant here, if $\tan\kappa_0 < 0$, λ is given by

$$\lambda_0 = \mathrm{i}\mu_0, \quad \mu_0\tanh(\mu_0\kappa_0) = -\tan\kappa_0, \quad \lambda_1 = 1, \quad \lambda_2, \ldots. \tag{67}$$

For example, if $\kappa_0 = \frac{3}{4}\pi$ and $\tan\kappa_0 = -1$,

$$\lambda_0 = \mathrm{i}1.016743, \quad \lambda_1 = 1, \quad \lambda_2 = 2.505496, \quad \lambda_3 = 3.893295, \quad \lambda_4 = 5.253502 \text{ etc.} \tag{68}$$

So for $\tan\kappa_0 < 0$, with the presence of diverging exponential terms,

$$y = a_0\,\mathrm{e}^{\mu_0\tau} + b_0\,\mathrm{e}^{-\mu_0\tau} + a_1\cos\tau + b_1\sin\tau + \sum_{n=2}^{\infty} a_n\cos(\lambda_n\tau) + b_n\sin(\lambda_n\tau). \tag{69}$$

The diverging exponential terms in the solution (69) corresponds to the instability of a mass-spring system when the mass is negative so that at an applied (or no) force, there is infinite displacement.

the trial solution

$$y = A\,\mathrm{e}^{\mathrm{i}\Omega\tau}, \quad v = B\,\mathrm{e}^{\mathrm{i}\Omega\tau}, \quad \phi = C\,\mathrm{e}^{\mathrm{i}\Omega\tau}\,. \tag{72}$$

Solving (71) with (72), we find

$$A = \frac{\tan\kappa_0}{\Omega\tan(\Omega\kappa_0) - \tan\kappa_0}, \quad B = \frac{-\mathrm{i}\tan(\Omega\kappa_0)}{\Omega\tan(\Omega\kappa_0) - \tan\kappa_0}, \quad C = \frac{\tan\kappa_0}{2\cos(\Omega\kappa_0)} \cdot \frac{1}{\Omega\tan(\Omega\kappa_0) - \tan\kappa_0}. \tag{73}$$

From here we can construct solutions for inhomogeneous terms $\cos(\Omega\tau)$ and $\sin(\Omega\tau)$ by taking the real or imaginary part of the solution (72) respectively. At resonance, when $\Omega\tan(\Omega\kappa_0) - \tan\kappa_0 = 0$, we take the trial solution

$$\begin{gathered} y = A\tau\,\mathrm{e}^{\mathrm{i}\Omega\tau}, \quad v = B\tau\,\mathrm{e}^{\mathrm{i}\Omega\tau}, \quad \phi = C\tau\,\mathrm{e}^{\mathrm{i}\Omega\tau} \\ \text{hence} \quad A = \frac{1}{\mathrm{i}\Omega}, \quad B = 1, \quad C = \frac{1}{\mathrm{i}\Omega\cos(\Omega\kappa_0)}. \end{gathered} \tag{74}$$

From (74), we see that the solution grows with time and secular terms appear.

C. Order ε^2 equation

Using (33), (34), (38), (39) and (40) with (42), we obtain

$$\begin{aligned}
&\frac{1}{\tan\kappa_0}\left[\tilde{\phi}_2'(\tilde{\tau}-\kappa_0) - \tilde{\phi}_2'(\tilde{\tau}+\kappa_0)\right] - \left[\tilde{\phi}_2(\tilde{\tau}-\kappa_0) + \tilde{\phi}_2(\tilde{\tau}+\kappa_0)\right] = \\
&-\frac{(\sigma\kappa_0)^2}{2}A_0\cos\kappa_0\cos\tilde{\tau} + \frac{(\sigma\kappa_0)^2}{2\tan\kappa_0}A_0\sin\kappa_0\cos\tilde{\tau} - \sigma\kappa_0 A_1\sin\kappa_0\cos\tilde{\tau} - \sigma\kappa_0 B_1\sin\kappa_0\sin\tilde{\tau} \\
&\quad - \sigma\kappa_0\frac{A_0^2\cos^2\kappa_0\tan\kappa_0}{2\pi}\sum_{n=1}^{\infty}\frac{2(2n+1)\sin(2n+1)\kappa_0\sin(2n+1)\tilde{\tau}}{\cos((2n+1)\kappa_0)\left[(2n+1)\tan((2n+1)\kappa_0) - \tan\kappa_0\right](n^2-\frac{1}{4})(n+\frac{3}{2})} \\
&-\frac{\sigma\kappa_0}{\tan\kappa_0}A_1\cos\kappa_0\cos\tilde{\tau} - \frac{\sigma\kappa_0}{\tan\kappa_0}B_1\cos\kappa_0\sin\tilde{\tau} \\
&\quad - \sigma\kappa_0\frac{A_0^2\cos^2\kappa_0}{2\pi}\sum_{n=1}^{\infty}\frac{2(2n+1)^2\cos(2n+1)\kappa_0\sin(2n+1)\tilde{\tau}}{\cos((2n+1)\kappa_0)\left[(2n+1)\tan((2n+1)\kappa_0) - \tan\kappa_0\right](n^2-\frac{1}{4})(n+\frac{3}{2})} \\
&- rA_1\cos\kappa_0\sin\tilde{\tau} + rB_1\cos\kappa_0\cos\tilde{\tau} - r\sigma\kappa_0 A_0\frac{\cos\kappa_0}{\tan\kappa_0}\sin\tilde{\tau} \\
&\qquad + r\frac{A_0^2\cos^2\kappa_0}{\pi}\sum_{n=1}^{\infty}\frac{\cos(2n+1)\tilde{\tau}}{\left[(2n+1) - \frac{\tan\kappa_0}{\tan((2n+1)\kappa_0)}\right](n^2-\frac{1}{4})(n+\frac{3}{2})} \\
&- \sigma A_1\cos\kappa_0\cos\tilde{\tau} - \sigma B_1\cos\kappa_0\sin\tilde{\tau} - \sigma^2\kappa_0 A_0\frac{\cos\kappa_0}{\tan\kappa_0}\cos\tilde{\tau} \\
&\qquad - \sigma\frac{A_0^2\cos^2\kappa_0}{\pi}\sum_{n=1}^{\infty}\frac{(2n+1)\sin(2n+1)\tilde{\tau}}{\left[(2n+1) - \frac{\tan\kappa_0}{\tan((2n+1)\kappa_0)}\right](n^2-\frac{1}{4})(n+\frac{3}{2})} \\
&+ \left[-A_1\cos\kappa_0\sin\tilde{\tau} + B_1\cos\kappa_0\cos\tilde{\tau} - \sigma\kappa_0 A_0\frac{\cos\kappa_0}{\tan\kappa_0}\sin\tilde{\tau}\right]2A_0\cos\kappa_0|\sin\tilde{\tau}| \\
&\qquad + \left[\frac{A_0^2\cos^2\kappa_0}{\pi}\sum_{n=1}^{\infty}\frac{\cos(2n+1)\tilde{\tau}}{\left[(2n+1) - \frac{\tan\kappa_0}{\tan((2n+1)\kappa_0)}\right](n^2-\frac{1}{4})(n+\frac{3}{2})}\right]2A_0\cos\kappa_0|\sin\tilde{\tau}| \\
&\qquad\qquad + \theta_1\sin\tilde{\tau}\cos\theta_0 + \theta_1\cos\tilde{\tau}\sin\theta_0
\end{aligned}$$

References

[1] D. K. Singh and S. W. Rienstra, "Nonlinear asymptotic impedance model for a Helmholtz resonator liner," *Journal of Sound and Vibration*, Vol. 333, No. 15, 2014, pp. 3536 – 3549.

[2] C. Bréard, A. Sayma, M. Imregun, A. G. Wilson, and B. J. Tester, "A CFD-based non-linear model for the prediction of tone noise in lined ducts," *7th AIAA/CEAS Aeroacoustics Conference*, 2001, AIAA-2001-2176.

[3] A. McAlpine, M. J. Fisher, and B. J. Tester, ""Buzz-saw" Noise: A Comparison of Modal Measurements with an Improved Prediction Method," *Journal of Sound and Vibration*, Vol. 306, No. 3-5, 2007, pp. 419–443.

[4] J. H. M. Disselhorst and L. van Wijngaarden, "Flow in the Exit of Open Pipes during Acoustic Resonance," *Journal of Fluid Mechanics*, Vol. 99, No. 2, 1980, pp. 293–319.

[5] S. W. Rienstra and A. Hirschberg, "An Introduction To Acoustics," Tech. rep., Technische Universiteit Eindhoven, 2012, revised and updated version of IWDE 92-06, `http://www.win.tue.nl/~sjoerdr/papers/boek.pdf`.

[6] T. H. Melling, "The Acoustic Impendance of Perforates at Medium and High Sound Pressure Levels," *Journal of Sound and Vibration*, Vol. 29, No. 1, 1973, pp. 1 – 65.

[7] H. H. Hubbard, editor, *Aeroacoustics of Flight Vehicles: Noise sources*, Aeroacoustics of Flight Vehicles: Theory and Practice. Volume 1 Noise Sources; Volume 2 Noise Control, Published for the Acoustical Society of America through the American Institute of Physics, 1991.

[8] A. S. Hersh, B. E. Walker, and J. W. Celano, "Helmholtz Resonator Impedance Model, Part 1: Nonlinear Behavior," *AIAA Journal*, Vol. 41, No. 5, 2003, pp. 795–808.

[9] C. K. W. Tam and K. A. Kurbatskii, "Microfluid Dynamics and Acoustics of Resonant Liners," *AIAA Journal*, Vol. 38, No. 8, 2000, pp. 1331–1339.

[10] C. K. W. Tam, K. A. Kurbatskii, K. K. Ahuja, and Jr. R. J. Gaeta, "A Numerical and Experimental Investigation of the Dissipation Mechanisms of Resonant Acoustic Liners," *Journal of Sound and Vibration*, Vol. 245, No. 3, 2001, pp. 545–557.

[11] C. K. W. Tam, H. Ju, M. G. Jones, and T. L. Parrott, "A computational and experimental study of slit resonators," *Journal of Sound and Vibration*, Vol. 284, 2005, pp. 947–984.

[12] J. M. Roche, L. Leylekian, G. Delattre, and F. Vuillot, "Aircraft Fan Noise Absorption: DNS of the Acoustic Dissipation of Resonant Liners," *15th AIAA/CEAS Aeroacoustics Conference*, 2009, AIAA Paper 2009-3146.

[13] C. K. W. Tam, H. Ju, M. G. Jones, W. R. Watson, and T. L. Parrott, "A Computational and Experimental Study of Resonators in Three Dimensions," *15th AIAA/CEAS Aeroacoustics Conference*, 2009, AIAA Paper 2009-3173.

[14] Q. Zhang and D. J. Bodony, "Numerical Simulation of Two-Dimensional Acoustic Liners with High Speed Grazing Flow," *AIAA Journal*, Vol. 49, No. 2, 2011, pp. 365–382.

[15] U. Ingard, "On the Theory and Design of Acoustic Resonators," *Journal of The Acoustical Society of America*, Vol. 25, 1953.

[16] S. W. Rienstra, "Impedance Models in Time Domain, Including the Extended Helmholtz Resonator Model," *12th AIAA/CEAS Aeroacoustics Conference, Cambridge, MA, USA*, 2006, AIAA Paper 2006-2686.

[17] R. M. M. Mattheij, S. W. Rienstra, and J. H. M. ten Thije Boonkkamp, *Partial Differential Equations: Modeling, Analysis, Computation*, Society for Industrial and Applied Mathematics, 2005.